Development of a small-scale actuator disk

Author
SANNE DE JONG HELVIG

Supervisor
R. JASON HEARST

December 11, 2019

NTNU – Trondheim
Norwegian University of
Science and Technology

Table of Contents

Figures

Abstract

The drag of a small-scale rotating wind turbine model was measured in a wind tunnel, and compared to the drag of different actuator disks, in order to find the actuator disk that most resembles the rotating model. The actuator disks were created with two different designs, one with uniform holes and one non-uniform, and three different solidities were used within each design. A solid actuator disk was also tested. The drag on the actuator disks were measured in the wind tunnel in the same matter as with the rotating model, using five different Reynolds numbers. When conducting the experiments, several measurements of the rotating models had to be conducted due to deviations in the measurement data. Some of these deviations were regarded as outliers and discarded, and the average was taken of the remaining measurements. This resulted in a drag coefficient profile which was compared to the drag coefficient profiles representing the different actuator disks. The disk with a non-uniform design and a solidity of 35% turned out to be the closest match, while the disk with uniform holes and a solidity of 35% was the second closest match. Assuming that the drag coefficient from the rotating model is correct and assuming a Gaussian distribution of the drag coefficients from the actuator disks, both of the disks with 35% solidity had the rotating models drag coefficient within its standard deviation, showing that it is reasonable to use these actuator disks to mimic the rotating model.

Acknowledgements

I would first and foremost like to thank my supervisor Jason Hearst, for always helping me out and supporting me, and for arousing my interest in aerodynamics in the first place. Through weekly meetings he has continued to push me and give me helpful input every step of the way, and he was always available when I needed som additional guidance.

I would also like to thank Magnus Kyrkjebø Vinnes, for helping me out whenever I got stuck and for his patience and positivity whenever we were troubleshooting. My thesis would not be what it is without your guidance.

I want to thank Lars Morten Bardal, for teaching me how to do calibrations, how to use the wind tunnel and for making the LabView program that he so kindly let me use.

I also want to give my thanks to Olav Rømcke, for teaching me how to use power tools, and the rest of Jason's Ph.D. students for all their helpful input at out weekly meetings.

Finally, I want to thank Adrian Bogen Skibelid, for proof reading, for all our sessions of throwing ideas back and forth, and for your continuous support.

Chapter 1

Introduction

In a world with a growing population, growing standards of living, and with it, a growing need for energy, simultaneous with an increasing focus on sustainability and environmentally friendly solutions, renewable energy has never been more relevant. The amount of onshore and offshore wind power is increasing, and numerous companies are working to find their role in the new market. Optimizing wind turbines and wind farms is an important aim, and researchers are using both simulations and experimental methods in order to explore different potentially efficient solutions.

However, within both methods, modeling a wind farm with moving blades is often extremely complicated. Thus, simplifications, such as the actuator disk, are commonly adopted. The idea of the actuator disk is that it produces the same drag as the wind turbine, resulting in similar bulk characteristics in the wake. The physical wind tunnel analogue to an actuator disk is a static, porous disk. However, at this point in time, there are no clear directions and no scientific consensus on how to design and make these porous disks in order to mimic rotating turbines when conducting experiments.

1.1 Problem formulation

The objective of the project described in this thesis is to develop a static, porous disk that has approximately matched characteristics to a small rotating wind turbine model provided by KTH, by matching the produced drag. In order to achieve this, the drag of the rotating wind turbine models are measured, and a variety of small-scale actuator disks are designed and 3D printed before drag measurements of the disks are conducted. Based on the results, the design will be honed in order to match the drag as closely as possible.

Chapter 2

Background

Within the field of wind turbine aerodynamics, the actuator disk theory describes the simplest way to model a rotating turbine. The actuator disk is a non-rotating disk, physically modeled as a static porous disk. The idea is that the actuator disk produces the same drag as a moving turbine, resulting in the same bulk characteristics in the wake.

The drag on the wind turbine models is the force in the direction parallel to the direction of the wind. The drag coefficient is further defined as

$$C_d = \frac{D}{\frac{1}{2} * \rho * u^2 * A} \tag{2.1}$$

where ρ is density, u is the flow velocity and A is the reference area.

The drag on an object changes as the velocity changes. According to theory, C_d increases as Re increases and then C_d levels of at $Re \simeq 10^3$, after which it remains approximately constant within the boundary of laminar flow. So this is the typical profile to expect when conducting drag measurements with varying Re. Here, Reynolds number is defined as

$$Re = \frac{\rho * u * L}{\mu} \tag{2.2}$$

where ρ is density, u is velocity, L is characteristic length and μ is the dynamic viscosity. For Reynolds number lower than $\simeq 5 * 10^5$ the flow is laminar, which is the type of flow relevant for this project.

The porosity is a measure of the permeable area of the disc and is defines as the ratio between the open area and the total area of the disc.

The renewed interest in wind energy originated in part from large funding programs by the American and European governments and from the realization that wind energy will be

a important contributor to production of affordable and clean energy in the next decades. A contribution to the overall electricity production of up to 20% is aimed by 2030, but to realize these targets, larger wind farms covering increasingly larger surface areas are required [14]. They wind turbines will grow not only in size, but also in capacity and money invested [3].

Current utility-scale turbines extend a significant distance into the atmospheric boundary layer, which is naturally turbulent [16] [13]. Further, placing the turbines in wind farms is the most economic and and efficient when it comes to planning, use of land and infrastructure, and maintenance [16]. Thus, wind turbines are permanently exposed to turbulence, either within the wind or when downstream turbines are hit by the turbulent wake created by upstream rows of turbines and their rotating turbine blades [16] [13].

Within a wind farm, as kinetic energy has been extracted from the wind and converted into electricity, the wind speeds do not recover to their freestream value after encountering the first row of turbines, and thus the wind speeds hitting subsequent turbines are lower than the freestream value [3]. Thus, the wake from the upstream wind turbines determine how much power a downstream turbine can generate and which mechanical loads it experiences, meaning that the study and characterization of wind turbine wakes has become an important research area. [16] [13] When turbine spacing and wind farm layouts are considered in a conventional approach, decisions are made based on the desire to limit the wake-induced fatigue loads on downstream turbines [14].

Variability in power output from wind turbines due to unsteady characteristics of the ABL is a challenge for the integration of large amounts of wind energy into the electricity grid, and the need for fill-in power and stronger components made to withstand unsteady loading turns the problem into that of a cost-minimizing problem, in order for wind energy to achieve the desired market share [5]

Studies of the interaction of large wind farms and the ABL, and how the wake develops and interacts with downstream WT arrays, are currently not prevalent, and improved knowledge and understanding of the interaction is necessary [14] [5] [18] [13] [1]. With improved understanding of this type of flows, wind farm developers can plan better-performing, less maintenance-intensive and longer-lasting wind farms, and manufacturers could create better fatigue load-mitigating designs [13].

Field tests are being carried out, but such approaches are expensive, difficult and by their nature incapable of being completely controlled [18]. Wind tunnel measurements have the advantage over full-scale experiments that the inflow and boundary conditions can be carefully controlled, and thus they can bring additional insight. [5]. Additionally, a wide range of inflow conditions can be tested and the created wake can be studied [18]. However, it should be mentioned that there is a need for increased amounts of data from actual wind farms, to evaluate whether experimental results are representative for the actual case.

A challenge for studying wind farms in wind tunnels is performing measurements with sufficiently high temporal and spatial resolution for a turbine array containing a large number of model turbines [5]. Therefore, small-scale turbines are relevant for experiments, and allow for extensive flow mapping studies to be conducted without the requirement of con-

structing scale turbines or the cost associated with large experimental test facilities[9]. The experts workshop organized by ForWind-Uni Oldenburg in 2018 on Wind Energy Science & Wind Tunnel Experiments agreed to qualify the smallest wind turbine models, with a rotor diameter less than 0.5 m, as wake-generating turbine models, independent on whether they are steady or rotating models [1].

However, using rotating blades for such small rotors, and building and operating 100 of them in a wind tunnel is not practical, but rather complex and costly. In addition, scaled rotating wind turbine models have inherent limitations since perfect flow similarity is not possible due to large scale differences. [5]. Rotating wind turbines can be compared to porous media due to their significant amount of flow-through. The question remains whether and to what extend it is possible to use simplified, non-rotating turbine models [16].

In order to study the wake, several numerical and physical modeling approaches are used. Some model the wind turbine with the simplest model, the AD concept, adding a drag source within the surface swept by the blades [2]. Porous disks are momentum sinks that does not directly extract energy from the flow, but instead dissipated kinetic energy of the incoming wind by generating small-scale turbulence in the near wake of the disk [12]. The simple but efficient actuator disk may be used as a simple method for simulating horizontal axis turbines.

Multiple experimental studies concerning ADs have already been conducted. Some are at the stage of developing the AD itself.

For example, Pierella and Sætran (2010) [17] studied the flow behind two circular grids of equal diameter and porosity but different mesh geometry. They used a biplane mesh, which turned out to produce a non-axisymmetric wake, and a monoplane mesh, giving an axisymmetric wake. The two wakes had different characteristics and the disks had different drags.

Earlier this year, nine research teams organized a round-robin measurement campaign of the wake of two porous discs in a homogeneous and low turbulent flow, performing similar wake measurements in different wind tunnels. [1] In general, results collapsed reasonably well across facilities.

Researchers such as Cannon et al. (1993) [8] have studied the wakes behind porous disks of varying solidity.

Others have gone further, and are moving towards the stage of using the actuator disks as simplifications for wind turbine models.

Bossuyt et al (2016) [5] used 100 porous disk models to model a wind farm in a wind tunnel at different layouts, in order to study power output variability and unsteady loading in a turbulent boundary layer.

Also [15] did analysis on the flow field around horizontal axis tidal turbines using mesh disks as rotor simulators.

In 1981, Sforza et al [18] used porous disks to simulate the effect of a wind turbine in

order to investigate the wake, using both experimental and numerical methods.

[16] investigated and compared an actuator disc and a model wind turbine exposed ti differnt uniform turbulent inflows, investigating the most variables. In the far wake, the wakes of both are similar. The results are independent on the inflow conditions. Velocity and turbulence intensity was different in the near wake.

A first requirement for a scaled wind turbine representation is a correct characterization of the wake structure (Theunisen et al 2015). When creating an AD to represent a WT, the starting point is often to match the diameter and the drag.

Studies conducted so far has a general agreement on the following terms. The near wake differs between the two models, as the turbulence in terms of the AD is produced by a grid, while rotating turbines introduce rotational momentum, tip and hub vorticies and turbulence from the blades (Zhang 2012). The difference in flow behaviour close to the model, especially prominent in terms of velocity deficit and turbulence intensity, is thus caused by fundamentally different turbulence production and mixing mechanisms, and leads to improper reproduction of the near flow [1].

However, blade signatures and rotational momentum have shown to be overshadowed by ambient velocity fluctuations in the far wake [2]. Porous disc models can create similar far wake as rotating models, making AD an adequate and appropriate substitution both at low and high inflow turbulence, typically from x/D = 3-4 [16] [1] [2] [11] [**?**] [**?**]. and thus the disks are acceptable when studying wake interactions at wind farm scale. Bossuyt et al 2016 concluded that the experimental setup of a model wind farm is able to capture the main trends in mean row power and unsteady loading, making it useful for layout optimization studies.

Studies have found that the drag coefficient is only weakly dependent on Reynolds number, so it remains roughly constant for a range of wind tunnel velocities. However, there is a dependence, meaning predictions of drag force with low levels of turbulence may differ from drag force experienced when operating in highly turbulent flow [4].

2.0.1 Experimentally

Lignarolo et al 2016 [12] provided an experimental analysis of the near-wake turbulent flow of a wind turbine and a porous disc. finding similarities and differences. They concluded that even in the absence of turbulence, the results show a good match in many variables such as thrust and energy coefficient, velocity, pressure and enthalpi. However, the turbulence intensity and turbulent mixing varied. The results suggested the possibility to extend the use of AD in numerical simulations until the very near wake, provided that turbulent mixing is correctly represented. The underlying question is how much the near wake differs given similarity of dimension, axial force and extracted energy. The stronger fluctuations in the WT wake are due to the pressence of concentrated tip vortices. They found the turbulence intensity of WT to be 2-4 times larger than for the AD wake in the near wake. Physics governing the turbulent mixing in the two wakes are intrinsically different. even in the absence of inflow turbulence, the velocity fields in the wakes are very

well comparable. Again, extend the use of AD in numerical simulations until the very near wake.

[12] also compared earlier experiments, showind a consistent decreasing drag coefficient with increasing porosity.

Also the other Lignarolo: [11] conducted an experiemtnal study focusing on the comparison between the wake of a turbine and an AD. WT wake caracterized by complex dynamics of tip vortex development and breakdown, and turbulent fluctuations. Wake of AD is instead characterized by isotropic random fluctuations. Looking into the limitations.

It is know that AD misestimates the effects of flow turbulence, due to the absence of the blade flow and its tip-vortes development and breakdown (Barthelie 2007). The mixing process across the wake interface and ultimately the rate at which the wake recovers the flow momentum is incorrectly modelled.

The far wake region is typically less affected by the presence of the rotating blades.

Despite the popularity of the simplified numerical model, few experimental studies are available., which analyse the flow field in he wake of an AD [11]. Matching the diameter and thrust coeff, the two give rise to the same wake expansion.

Blackmore et al [4] used experiments to investigate the effects of turulence on the drag of solid discs and porous disc turbine simulators.

Aubrun et al (2013) [2] studied wind turbine wake properties, by comparing a non-rotating simplified WT, based on the AD concept, and a rotating model, to determine the limits of the simplified model to reproduce a realistic wake. Concluding that the wakes, in the modeled ABL, were indistinguishable after 3D downstream. (in relatively high turbulent inflow conditions. Discrepancies still exist at x/d = 3 in low turbulent inflow conditions, but are relatively minor. So the simplified AD model seems to be usable to reproduce the far wake.

2.0.2 Use in CFD simulations

Numerical simulations and experimental studies can compliment each other for a better understanding.

As mentioned, wind turbines are large, on the order of hundreds of meters, with a typical spacing within a farm of 5-10 D, and a thickness of the blade on the order of 1m. In order to resolve the full turbine geometry, ideally one would need to build a mesh with sub-milimeter resolution in the blade BL inside a kilometer-scale computational box within the entire farm fits. As a consequence, we use a simplification: a model with an accuracy that generates the correct velocity deficit and TI in the far wake while ensuring that it is not too computanionally demaning. Thus, most codes rely on AD. [13] [10] [9] Such models are an attractive alternative, as they require fewer grid cells and not as small grid dimensions, allowing larger time steps. This efficiency comes at the expense of resolving the fine details of the blade BL, but if the objective is the far wake, this trade off is reasonable and AD is more than acceptable. As with experiments, a porous disc with the same diameter that applies a similar thrust force upon the moving fluid as a set of rotating blades may be

used, but turbulence structures shed from the disk vary compared to the rotor in the near wake. Thus, AD is well suited for full wind farm computations. And work is being done in developing these models and comparing them to experimental results [9] [13], including a organized workshop to compare different state-of-the-art numerical models for the simulation of wind turbine wakes [10], especially comparing wakes produced from simulations to those produced with experiments.

Also on the computational area, more work related to AD is needed. For example, [13] claims the need for implementing a model for the wind turbine towel and nacelle to assess their impact on the turbine performance and wake profile.

Obtaining both real and experimental data is necessary in order to develop simulation methods and check simulated observations and predictions against actual wake characteristics. Experiments also provide data for computational model validation and for comparison for future work.

However, with such further development, a relatively inexpensive tool for assesment of flowfields and planning of wind farms would be at hand for the industry (to enable the industrial use of CFD), and the CFD AD could be an accurate and validated method for numerically modelling turbines [18] [9].

2.0.3 Developing the actuator disk

One main issue remains, as there is no standard for designing and making the experimental actuator discs. Bossuyt et al (2016) [5] used a symmetric design, with a solidity that decreases with radial direction. Lignarolo et al (2016) [12] used a layered fine metal mesh, considered as a grid turbulence generator, while Aubrun et al [2] used fine metal meshes with varying porosity at the center of the disc and at the outer edge. Blackmore et al (2013) [4] used a hole pattern to maintain approximately uniform porosity across the radius. Aubrun et al [1] used both a metallic mesh with uniform porosity and a porous disc of plywood with radially non-uniform porosity. Sforza et al (1981) [18] used perforated metal plates, while Pierella and Sætran [17] used wooden grids. Myers et al (2010) [15] used PVC plastic for their discs. Even though the simulated turbine will vary, and thus the diameter, porosity and drag coefficient of the disc, a standard design creating the desired wake would be practical to create uniformity and comparability between experiments, and to save time so that every researcher around the world does not need to start the phase by developing their own disk.

Neunaber [16] cut her disk from an aluminium plate in a non-uniform matter. She also highlited that she had a 100% blockage in the center, where the nacelle is located in the case of a turbine, and that blackage shoul vary linearly similar to a real turbine.

Another detail to take into consideration at this point is the wind-tunnel blockage efffects created by the turbine models which may affect the wake. Thus, it is desired for the discs to be small [18].

Also wanted further work, as to explain why a smaller diameter porous disc resulted in lower drag coeff than the larger diameter disc with same porosity. [4]

Nevertheless, in a direct experimental comparison of turbulent flow in the near wake, a porous disk (with same dimention and axial force as a rotating turbine) is currently not available [12]. Main drivers are porosity, structural stiffness, wake-flow uniformity

Chapter 3

Method

In the following, the experimental setup will be explained. A short description of the Rotating wind turbine model (RTWM)s that were used will be given, followed by an explanation of the process of designing and creating the ADs. How the drag measurements in the wind tunnel were conducted and possible sources of uncertainty that occurred during the testing will also be highlighted. Finally, a summary of how the data was processed and how the calculations were conducted to find C_d will be given.

3.1 Experimental setup

In order to measure the drag on the RTWM and the ADs, a wind tunnel and a force plate is needed as part of the experimental setup. There was also the need to construct a test rig on which the models could be placed inside the wind tunnel.

3.1.1 Force plate, wind tunnel and associated equipment

The wind tunnel being used is $1\ \mathrm{m}$ wide and a 0.5 m tall. It has a maximum velocity of 35 m/s. The turbulence intensity is unknown, however it will be found when doing Particle Image Velocimetry (PIV) measurements in future work. Equipment can be placed inside the wind tunnel by removing a glass window which is 75 cm wide and 35 cm tall. The wind velocity is changed by manually turning a wheel, that in turn changes the position of the valves next to the motor inside the tunnel. At the floor of the tunnel there is a small hole, making it possible to connect the item one is measuring forces on inside the tunnel to the load cell underneath the tunnel.

Underneath the wind tunnel is a force plate of the type AMTI BP400600HF 1000, able to measure the force and moment components along the x-, y- and z-axes. The force plate has an accuracy of ...

The drag measured by the load cell is sent as a voltage signal through an amplifier. Afterwards, it is sent through a low pass filter, with a cut-off frequency of 1000 Hz. The data was gathered and saved using LabView, and the signal was turned back into a force using the given relationship between voltage and newton.

Inside the tunnel there is a sensor measuring the temperature, and a pitot tube measuring the pressure. The signal from the pitot tube is used to quantify the wind velocity.

A potential uncertainty related to the wind tunnel is the fact that the pitot tube is placed in the vertical center of the tunnel, about 4 m upstream of the Wind turbine model (WTM)s. Thus, the velocity measured is not necessarily the same as the velocity that hits the WTMs, which are placed close to the floor of the tunnel. Due to the development of wall boundary layers, the velocity hitting the WTMs is likely lower than the measured and registered velocity.

3.1.2 The rig

The test rig consisted of a magnetic steel bar of 0.5 m stretching across the width of the wind tunnel, on top of an aluminum cylinder which connects the bar to an aluminum plate, that in turn can be strapped to the load cell underneath the wind tunnel. Thus, the aluminum cylinder went through the hole at the bottom of the wind tunnel, and then the rest of the hole was covered with tape. Careful consideration was taken when adding the tape, so that the aluminum cylinder did not touch anything, as that would affect the force measurements.

The bar was lifted about 1 cm above the ground floor of the wind tunnel. Initially, it was desired to have the steel bar be almost as long as the width of the wind tunnel, in order to avoid affecting the flow outside of what is already the boundary layer in the tunnel. Similarly, it was desired to have the hub of the turbines exactly in the vertical middle of the tunnel to avoid the boundary layers. However, this was not doable. The hole in the bottom of the wind tunnel was limited in size, which meant that the steel bar could only be connected to the load cell underneath the tunnel through one aluminum cylinder with a small diameter of about 2 cm, making the support less robust. The length of the metal bar had to be shortened, and the bar had to be brought closer to the tunnel floor, in order to avoid bending and flapping at the ends.

3.2 Wind turbine models

The two-bladed rotating WTMs are the property of KTH in Stockholm, and can be seen in figure 3.1. They have a diameter of 45 mm, and a hub height of approximately 65 mm. Magnets are incorporated into the bottom of the models.

Figure 3.1: One of the rotating models.

3.3 The actuator disks

As mentioned, there is no standard way of designing ADs. For this project, it was desirable to create ADs with multiple solidities, and a possible method was to create two ADs that are connected and can be rotated relative to each other, in order to change the solidity. However, this seemed hard to achieve at such small scales. In addition, the author was skeptic to the method based on the results of Pierella et al (2010) [17], showing that a monoplane and a biplane AD made with the same diameter and porosity produced different drags, making the cases not comparable. Since making a monoplane disk is probably simpler and easier to recreate, this method was preferred.

3.3.1 Computer-aided design and 3D printing

The ADs, as well as their towers, were designed using SolidWorks. Cura was used to turn the designs into readable code for the 3D printers, and the parts were then printed using a printer of the type Ultimaker 2+. The material used was PLA.

A significant limitation occurred during the design process. The 3D printers available could not print thinner than 0.4 mm, meaning that each line in the disks had to be at least 0.4 mm. However, printing lines of 0.4 mm proved troublesome, and it was decided that all lines should be equal to or thicker than 0.5 mm. This is significant given that the disks are in themselves of such small dimensions. So there turned out to be a limit to how porous the disks could be made.

Figure 3.2: The 3D printed tower.

3.3.2 Design of the tower

The tower was designed to have the exact same dimensions as the given RTWM's tower. Most importantly, it had a hub height of 65 mm. Underneath the base there was made a hole that could fit a cylindrical neodymium magnet with a diameter of 10 mm, a height of 2.5 mm and a strength of 0.9 kg. The ADs were made to be interchangeable, and thus the end of the tower where the ADs would be connected was made slightly thinner in order to fit into the designated holes in the ADs. Three towers were printed, and one of them can be seen in figure 3.2.

3.3.3 Actuator disk design

The ADs were designed with a diameter of 45 mm, to match the RTWMs. The disks were 2.5 mm thick.

Two different designs of ADs were tested. The first has numerous equally-sized holes spread symmetrically around the center point of the disk, as seen in figure 3.3a and 3.4a. It is quite similar to the design of Blackmore et al (2013) [4]. The design is also meant to be similar to those AD designs that consist of a thin metal grid, comparable to a grid turbulence generator, as used by Aubrun et al (2013) [2] and Lignarolo et al (2016)[12]. This design will be called Uniform Holes Disk (UHD) going forth. The second design is also symmetric around the center point, but this one has rectangular holes that vary in size with radial distance, increasing in size as the radial coordinate increases, as seen in figure 3.3b and 3.4b. Thus, the solidity decreases with radial coordinate, matching the characteristics of an actual WT. This design was used by Camp and Cal (2016 and 2019)

[6] [7] and by Neunaber [16]. This design will be called NUD.

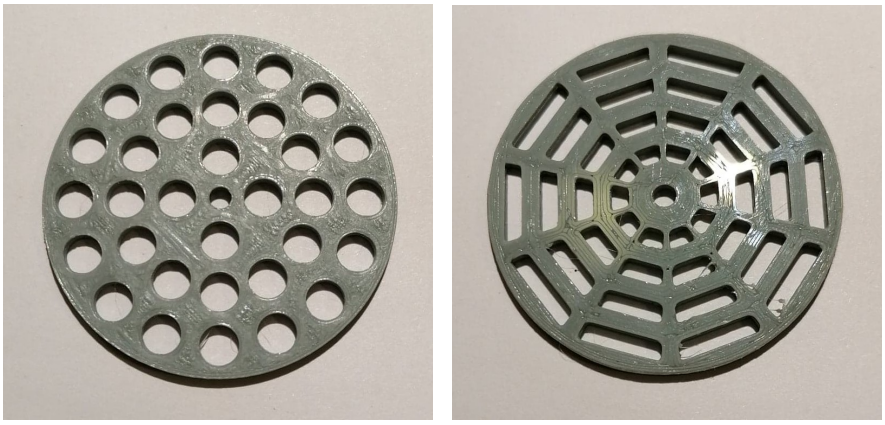

(a) The UHD design **(b)** The NUD design

Figure 3.3: ADs with a solidity of 60%.

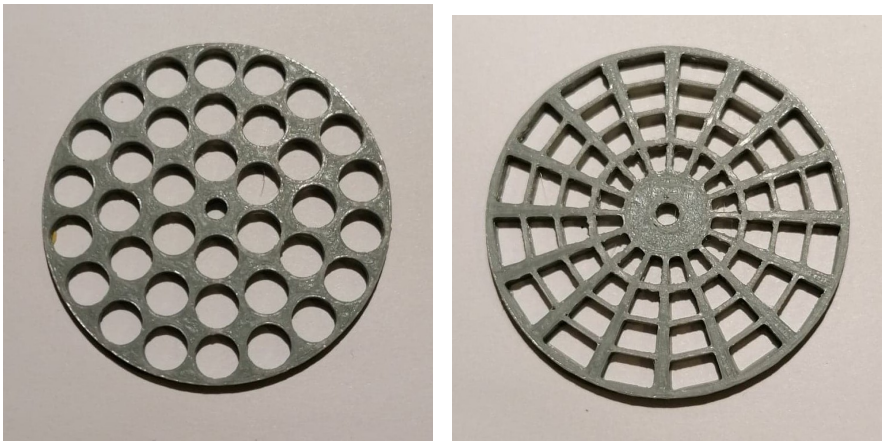

(a) The UHD design **(b)** The NUD design

Figure 3.4: ADs with a solidity of 40%.

For each of these configurations, two solidities were created as an initial try. The chosen values were 60% and 40%. A solid disk was also made and tested as a reference case. Three disks of each design and solidity were printed.

Based on the resulting drag profiles from the initial round of testing, two sets of ADs with a solidity of 35% were designed and made, which can be seen in figure 3.5a and 3.5b. The first was made based on the UHD design. Due to the mentioned limitations regarding the printing thickness, providing a solidity less than 39% with this design proved problematic. Hence the design was slightly changed, allowing for the holes to also cover the edges of

the ADs. It was kept in mind that this results in a different disk circumference, and that this might result in a drag force that is not directly comparable to the drag of the previously tested disks with UHD design. The second disk was made using the NUD design.

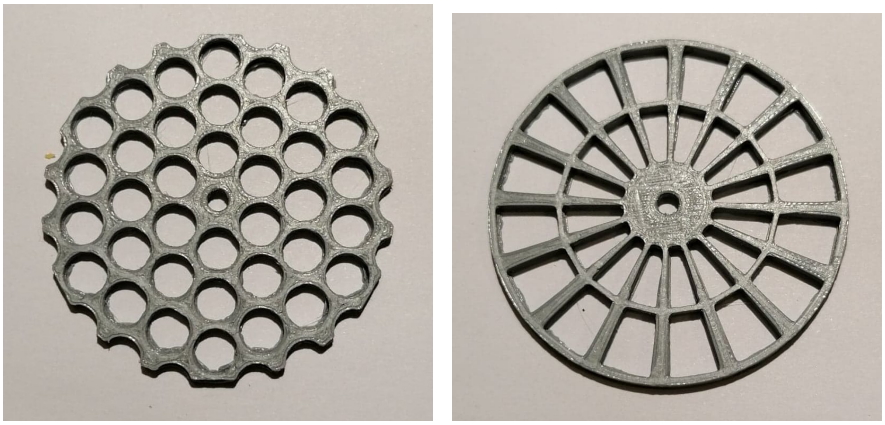

(a) The UHD design **(b)** The NUD design

Figure 3.5: ADs with a solidity of 35%.

Each disk was as mentioned made with a small hole in the center, used to connect the disks to the tower. Thus, this hole was filled in during the tests in the wind tunnel, and did not affect the solidity. This connection resulted in a larger solidity in the center of the disks, which can be argued to represent the nacelle of a wind turbine. A disk connected to a tower can be seen in figure 3.6.

Figure 3.6: The 3D printed tower connected to the 3D printed NUD disk with 35% solidity.

3.4 Testing

Given that the size of the WTMs was quite small, the models were tested in the wind tunnel three at a time, to ensure that the drag would be of an order that the instruments were able to measure and of an order where slight changes in the design resulting in slight changes in drag would be noticeable. The WTMs were placed along the steel bar such that one model was in the center of the tunnel, and the other two were placed symmetrically on each side, with a distance of 4D between them.

Even though the RTWM were magnetic, it proved problematic to make them stay in the same position, with the turbine perpendicular to the incoming flow direction, especially as the wind velocity increased. Thus, the rotating models were connected to the steel bar using small pieces of tape. The 3D printed towers were able to stay in the right position on the base by themselves. Still, they were taped to the base like the RTWMs, to make sure the cases were comparable.

As the drag is the only force of interest in this work, only the force in the x-direction is measured. The force was measured for five different wind velocities; 5 $\mathrm{m\,s^{-1}}$, 7.5 $\mathrm{m\,s^{-1}}$, 10 $\mathrm{m\,s^{-1}}$, 12.5 $\mathrm{m\,s^{-1}}$ and 15 $\mathrm{m\,s^{-1}}$. This corresponds to Reynolds numbers 14 860, 22289, 29 719, 37149 and 44 579, respectively, so all of the order 10^4. When calculating Reynolds number, the characteristic length used is the diameter of the ADs, 0.045 m. Since the velocity was changed by manually turning a wheel, a slight difference in the velocities occurred between the different measurement sets.

The force plate drifted over time, as is often the case with force measuring equipment.

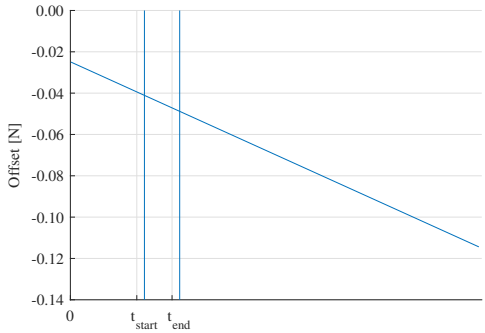

Figure 3.7: The approximated drift between the two zero measurements. t_{start} indicated where the 60 s measurement started, and t_{end} indicated where the measurement ended.

To take this into consideration when measuring the forces, zero measurements were conducted before and after every measurement. A 20 s tare measurement was first conducted. The wind tunnel was then turned on, with the velocity initially set to about 1 $\mathrm{m\,s^{-1}}$, and then turned up to the desired value. A measurement lasting 60 s was then conducted. The velocity was once again reduced to about 1 $\mathrm{m\,s^{-1}}$, and the wind tunnel was shut off. After the wind tunnel had quiet down and there was close to no moving air inside, another 20 s tare measurement was conducted. The wind tunnel needed about 10 min before one could be sure that the air inside was still, meaning that the measurements were quite time consuming. When measuring, a sampling rate of 1000 Hz was used.

Besides measuring the drag on the RTWMs and on all the different sets of ADs, a measurement set was also conducted having only on three towers on the base, without having any disks connected to them. Thus, the drag of the base and the towers was quantified.

3.5 Calculations

For each WTM at each wind velocity, the data collected from the wind tunnel consisted of a time series of voltages corresponding to the measured drag force and the measured wind velocity, as well as the points in time when the first zero measurement and the second zero measurement were conducted and when the 60 s drag measurement started. Using Matlab, this data was treated.

The force plate was assumed to drift linearly. Thus, using the two zero measurement values, a linear function approximating the drift was created. The part of this linear function corresponding to the 60 s where the force measurement was conducted, was extracted, as seen in figure 3.7. For each measured force in the time series, the corresponding drift was subtracted. After, the average drag force over the time series was calculated, as well as the variance and standard deviation.

In the same matter, the drift was subtracted and the average drag force was calculated for the measurements that were conducted using only the base and the tower, for each of the different wind velocities. These average drag forces were then subtracted from the

averages drag forces calculated earlier for all the different WTMs, so that what remains is only the drag on the disks or the turbine blades, excluding the towers and the base.

Finally, this calculated drag was divided by three, so as to only consider the drag on one disk or one set of rotating blades. This force was further used in calculating the drag coefficient, using equation 2.1, together with the total swiping area of the rotating turbine model, being πr^2.

Another value collected as part of the measurement data was the average temperature during the 60 s of measuring. This was used to decide on the appropriate value for the air density, ρ, and air dynamic viscosity, μ, when calculating the drag coefficient and the Reynolds number. However, the temperature only varied between about 20°C and 23°C. Since this variation is fairly small, it was assumed to not have any significant impact on the resulting drag.

Chapter 4

Results & Discussion

During the measurement phase, it turned out that several measurement sets needed to be conducted for the rotating models, due to several deviations in the data. In this section, the measurement data and the process of treating it will be presented, together with the final average drag coefficient of the rotating models. After, the drag and drag coefficient of all the different ADs will be presented and compared to the average results for rotating models.

4.1 Rotating models

The first measurement set conducted using three RTWMs resulted in a drag coefficient that seemed relatively independent of Reynolds number for four of the measured wind velocities, but with a noticeable deviation at $Re \approx 1.5 * 10^4$. To investigate whether this deviation was due to a measurement error, a second measurement set was conducted, this time using three new RTWMs. This second measurement gave more of an expected result at $Re \approx 1.5 * 10^4$, however showed a deviation at $Re \approx 4.5 * 10^4$. Due to continuous deviations, however differing in size and appearing at different velocities, six measurements were eventually conducted. They were all done with different sets of RTWMs, except for measurement set three and four, which were done using the same set of models. The resulting drag coefficients can be seen as a function of Re in figure 4.1.

As can be seen, there is some variation between the different measurements. The drag coefficients resulting from the third and the fourth measurement set, conducted using the same models, are quite similar at $Re \approx 1.5 * 10^4$, $Re \approx 2.3 * 10^4$ and $Re \approx 3.7 * 10^4$, and at $Re \approx 4.5 * 10^4$, they completely overlap. This seems to show that the measurement is to some degree repeatable, and that one of the reasons for the varying results is simply that there are small differences between the RTWMs. These differences can for example be related to the friction between the rotating blades and the hub that they rotate around. In addition, the blades stay onto the hub due to a small piece of see-through plastic, that

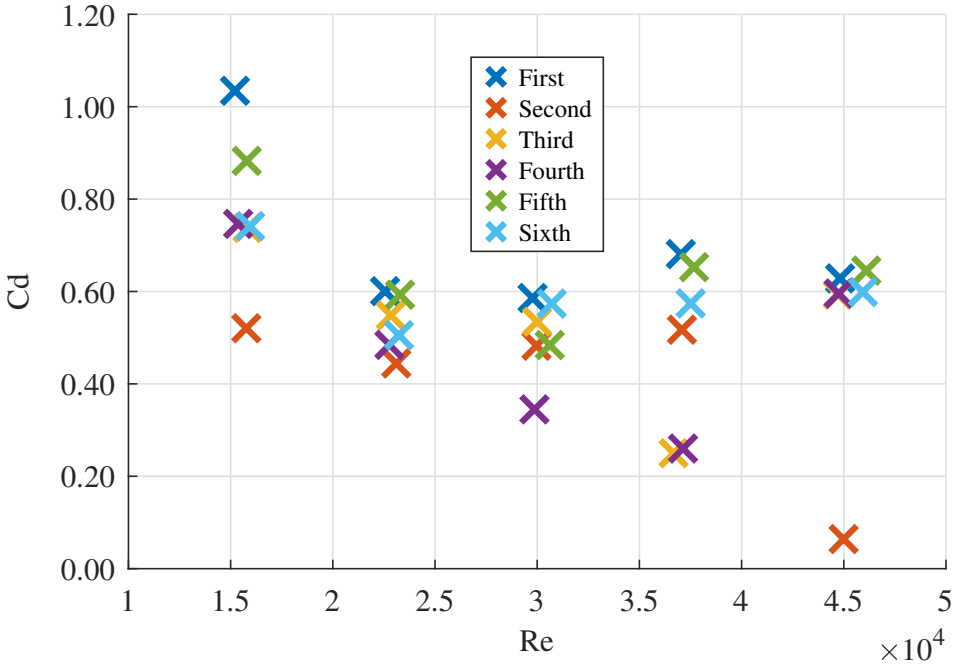

Figure 4.1: The drag coefficient for the rotating models, obtained through six rounds of measurements.

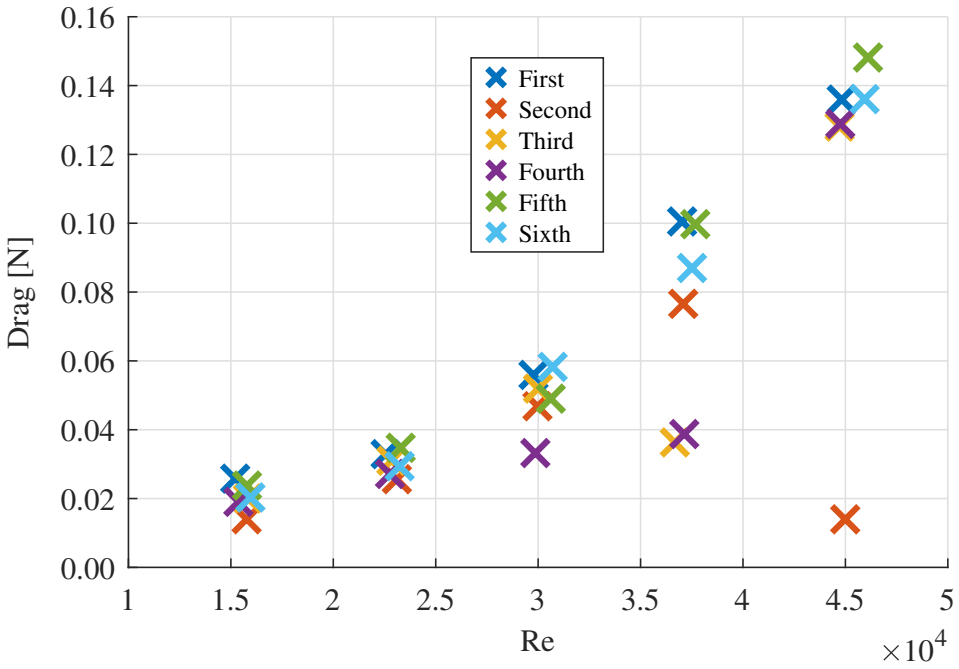

Figure 4.2: The measured drag for the rotating models, obtained through six rounds of measurements.

differs in size between the models. If it is too big, it might fasten the blades too tightly, causing added friction. If it is too small, the blades might be too loose, and they may start to oscillate. These types of differences were evident during the measurement phase, as several times the measurements had to be stopped midway due to one of the turbines suddenly not rotating anymore, and once because the rotating blades fell of the model.

However, even between the third and fourth measurement set, there is a noticeable difference at $Re \approx 3 * 10^4$, showing that differences between the RTWMs is not the only cause for the varying results. Other possible causes of this variation may be related to fluctuations in the applied wind velocity and to noise in the transducer and the electrical equipment used. Human error is also an important factor, as the models were placed in the wind tunnel by hand, and the turbine blades were not necessarily always exactly perpendicular to the incoming flow direction.

To investigate the results further, the drag resulting from the different measurements were plotted as a function of Reynolds number, as seen in figure 4.2.

The drag at $Re \approx 4.5 * 10^4$ is significantly lower than the drag at $Re \approx 3.7 * 10^4$ for the second measurement set. The same is the case for the third measurement set, where the drag at $Re \approx 3.7 * 10^4$ is significantly lower than the drag at $Re \approx 3 * 10^4$. This is not physical, and thus these to measurements are assumed to be outliers.

The measurements at $Re \approx 3.7 * 10^4$ were studied further. The average drag of the measurements that seem to cluster is 0.091 N, with a standard deviation of 0.0114 N. Looking at the measurement value from the fourth measurement set, it has a drag of 0.0387 N at this Re, and thus it is over four standard deviations away from the mentioned average. Hence, this value is considered to be an outlier. (It is worth noting that this outlier coincides with the already discarded drag measurement from the third measurement set. For these two measurement sets, using the same set of rotating models, there seemed to be considerably large amounts of noise on the signal for velocities between 11 $\mathrm{m\,s^{-1}}$ and 13 $\mathrm{m\,s^{-1}}$, which might explain this repeated deviation.)

A similar study was conducted for $Re \approx 3 * 10^4$. Five of the measurements seem to coincide, with an average drag of 0.0524 N and a standard deviation of 0.0047 N. The drag resulting from the fourth measurement set is 0.0332 N, and thus more than four standard deviations away from the average. Hence, this value is also considered to be an outlier.

In total, four measured drags has been discarded, and the four associated drag coefficients were removed. In order to achieve a representative value for the drag coefficient of the RTWMs, the average of the remaining drag coefficients was taken at each velocity. This resulted in the drag coefficients seen in figure 4.3. It is assumed that the drag measurements have a Gaussian distribution about some mean value, and that this calculated average based on six measurements is representative for the average one would have gotten if all the rotating models had been testes and all the tests had been conducted multiple times.

4.2 Drag on the actuator disks

The drag and the drag coefficient measured on the produced ADs have been studied. The solid disk, used as a reference case, produced the drag seen in figure 4.4a and the drag coefficient seen in figure 4.4b. Further, the drag and the drag coefficient for the two types of disks with 60% solidity can be seen in figure 4.5a and 4.5b, respectively.

The drag for the disks with 40% and 35% solidity were plotted in figure 4.6, and the drag coefficient for the same disks were plotted in figure 4.7. As these disks produced a drag fairly close to the average drag of the RTWMs, the average drag and drag coefficient representing the rotating models is also included in the plots, to ease the comparison.

Some general trends can be observed from these graphs. For all the AD and RTWM measurements, the drag is seen to increase with increasing Re, as one would expect. Another trend that can readily be seen, is that the drag coefficient decreases with decreasing solidity. This coincides with what has been found in the literature. Lignarolo et al (2016) [12] presented a comparison between different drag coefficients as a function of solidity, based on the results presented in six different papers. Compared, the ADs used in this current study results in a slightly higher drag coefficient for all the solidities. This can be caused by differences in inflow conditions, such as inflow turbulence, or be due to the models being placed in the boundary layer in this study, in contrast to most cases in literature where the hub is in the free stream flow. However, Lignarolo et al also concludes that the drag

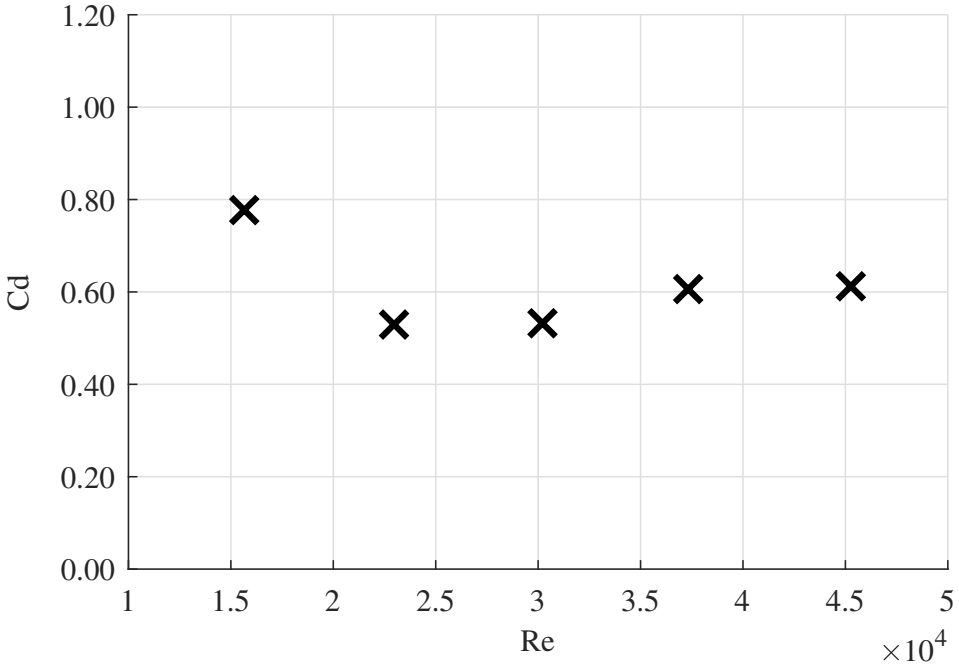

Figure 4.3: The average drag coefficient for the rotational models at each wind velocity, based on the six conducted measurements, after removing the assumed errors and outliers.

coefficient seems to be approximately linearly decreasing with decreasing solidity, which is the case with the current measurements as well.

For all the different ADs and for the RTWMs, the drag coefficient corresponding to $Re \approx 1.5 * 10^4$ is significantly higher than for the other Reynolds numbers, while the drag coefficient related to the other four Reynolds numbers generally seem to concentrate around some mean value. This deviation at $Re \approx 1.5 * 10^4$ does not appear in the experiments of Blackmore et al (2013) [4], who uses the same range of Re as in the present study. Thus, the deviation is most likely due to measurement noise. When studying the standard deviation for each 60 s measurement, the standard deviation is always between 0.011 and 0.015, independent of which disk is being studied, showing that this is probably be the size of the measurement noise related to the transducer and electrical equipment. The drag force at such a low velocity will be quite small, and it seems that the measurement noise is larger than the actual drag and interfering with the measurements. However, this result will not have any significant impact on the future work, as the future work will focus around Reynolds numbers higher than $Re \approx 1.5 * 10^4$.

Looking at figure 4.7, the NUD with 35% solidity and the UHD with 35% solidity seem to best match the drag of the rotating model. To study this further, the average drag coefficient over the four Reynolds numbers where the measurements already seem to gather around some mean, is calculated, and presented in table 4.1. The standard deviation is also

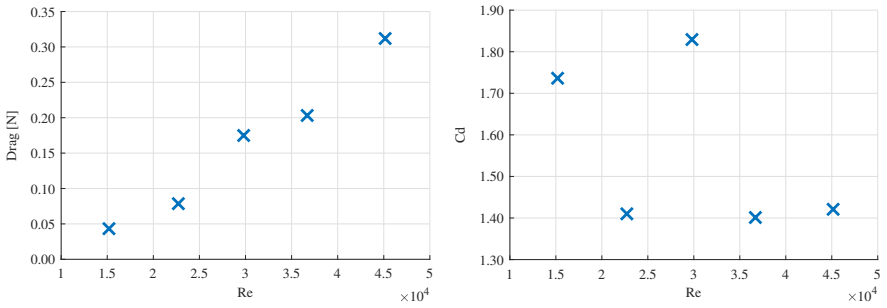

(a) The drag. **(b)** The drag coefficient.

Figure 4.4: Using the solid disk.

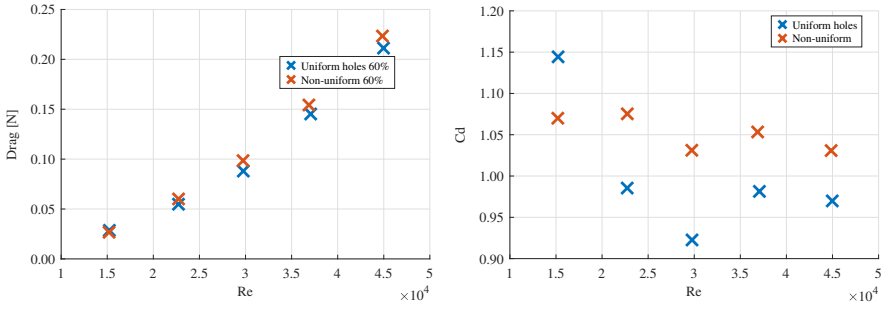

(a) The drag. **(b)** The drag coefficient.

Figure 4.5: Using the disks with 60% solidity.

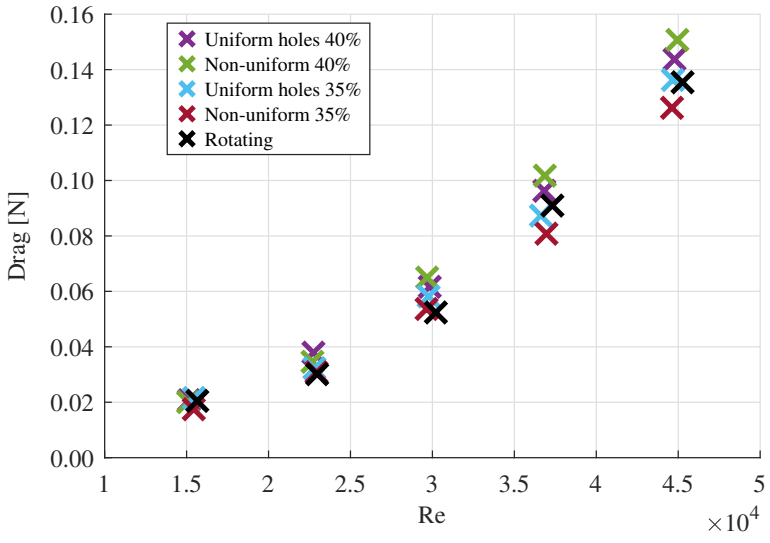

Figure 4.6: The drag for the disks with 40% and 35% solidity, compared to the average drag coefficient of the rotating disks.

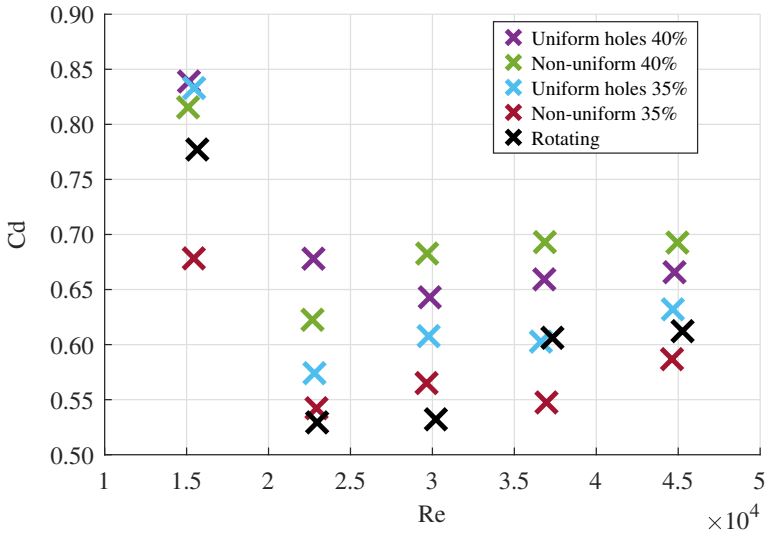

Figure 4.7: The drag coefficient for the disks with 40% and 35% solidity, compared to the average drag coefficient of the rotating disks.

Disk type	Average Cd	Cd standard deviation
Rotating average	0.570	-
Uniform holes, 40%	0.662	0.053
Non-uniform, 40%	0.673	0.057
Uniform holes, 35%	0.604	0.051
Non-uniform, 35%	0.560	0.051

Table 4.1: Average Cd for the rotating model and the disks with 35% solidity.

included, as well as the average Cd and the standard deviation for the 40% ADs. If one assumes that the Cd corresponding to the rotating model is correct, and that the ADs have a Gaussian distribution, is can be seen that the standard deviation of both disks with 35% solidity covers the rotating Cd value, while neither of the 40% solidity disks do. Thus, it is concluded that the disks with 35% solidity is the best match, and based on the averages it seems that the NUD with 35% solidity is the closest match, while the UHD with 35% solidity is the second closest.

An additional remark that can be made related to the measurements is that there does not seem to be any clear trends regarding the drag coefficient when using the NUD design compared to when using the UHD design.

Chapter 5

Future work

As concluded in [], in order to create an AD matching a RTWM, the wake must be similar. Matching the drag coefficient is only the first step in this process.

Going forth, the rotating models and the two ADs with the closest matching drag coefficient will be studied using Particle Image Velocimetry. Thus, both the flow in front of the models and the wake behind the models can be studies. This method can be used to examine the velocity deficit and the turbulence intensity in the wake, amongst others. It is also desired to integrate the wake in order to find and compare the axial induction factor.

Further, the plan is to acquire 100-150 RTWMs, and set them up as a wind farm in a larger wind tunnel. Equally many ADs will be made, using the design that most closely match the drag and the wake, and they will also be set up as to simulate an entire wind farm. This will be done in order to study the similarities and differences between the models when used for wind farm modelling, to some extent determine the suitability of using ADs when modelling large wind farms.

Chapter 6

Conclusion

Bibliography

[1] S. Aubrun, M. Bastankhah, R.B. Cal, B. Conan, R.J. Hearst, D. Hoek, M. Hölling, M. Huang, C Hur, B. Karlsen, I. Neunaber, M. Obligado, J. Peinke, M. Percin, L. Saetran, P Schito, B. Schliffke, D. Sims-Williams, O. Uzol, M.K. Vinnes, and A. Zasso. Round-robin tests of porous disc models. *Journal of Physics: Conference Series*, 1256:012004, jul 2019.

[2] S. Aubrun, S. Loyer, P. Hancock, and P. Hayden. Wind turbine wake properties: Comparison between a non-rotating simplified wind turbine model and a rotating model. *Journal of Wind Engineering and Industrial Aerodynamics*, 120:1–8, 09 2013.

[3] R. J. Barthelmie and L. E. Jensen. Evaluation of wind farm efficiency and wind turbine wakes at the nysted offshore wind farm. *Wind Energy*, 13, 04 2010.

[4] Tom Blackmore, William Batten, Gerald Muller, and AbuBakr Bahaj. Influence of turbulence on the drag of solid discs and turbine simulators in a water current. *Experiments in Fluids*, 55, 12 2013.

[5] Juliaan Bossuyt, Michael Howland, Charles Meneveau, and Johan Meyers. Measurement of unsteady loading and power output variability in a micro wind farm model in a wind tunnel. *Experiments in Fluids*, 58, 12 2016.

[6] Elizabeth Camp and Raúl Bayoán Cal. Mean kinetic energy transport and event classification in a model wind turbine array versus an array of porous disks: Energy budget and octant analysis. *Physical Review Fluids*, 1:044404, 08 2016.

[7] Elizabeth Camp and Raúl Bayoán Cal. Low-dimensional representations and anisotropy of model rotor versus porous disk wind turbine arrays. *Physical Review Fluids*, 4, 02 2019.

[8] S. Cannon, F. Champagne, and A. Glezer. Observations of large-scale structures in wakes behind axisymmetric bodies. *Experiments in Fluids*, 14:447–450, 05 1993.

[9] M.E. Harrison, William Batten, Luke Myers, and AbuBakr Bahaj. Comparison between cfd simulations and experiments for predicting the far wake of horizontal axis tidal turbines. *Renewable Power Generation, IET*, 4:613 – 627, 12 2010.

[10] Lorenzo Lignarolo, Dhruv Mehta, Richard Stevens, Ali Yilmaz, Gijs Kuik, Søren Andersen, Charles Meneveau, Carlos Ferreira, Daniele Ragni, Johan Meyers, Gerard van Bussel, and Jessica Holierhoek. Validation of four les and a vortex model against stereo-piv measurements in the near wake of an actuator disc and a wind turbine. *Renewable Energy*, 94:510–523, 08 2016.

[11] Lorenzo Lignarolo, Daniele Ragni, Carlos Ferreira, and Gerard van Bussel. Kinetic energy entrainment in wind turbine and actuator disc wakes: An experimental analysis. *Journal of Physics: Conference Series*, 524:012163, 06 2014.

[12] Lorenzo Lignarolo, Daniele Ragni, Carlos Ferreira, and Gerard van Bussel. Experimental comparison of a wind-turbine and of an actuator-disc near wake. *Journal of Renewable and Sustainable Energy*, 8:023301, 03 2016.

[13] Luis Martínez Tossas, Matthew Churchfield, and Stefano Leonardi. Large eddy simulations of the flow past wind turbines: actuator line and disk modeling: Les of the flow past wind turbines: actuator line and disk modeling. *Wind Energy*, 18, 04 2014.

[14] Johan Meyers and Charles Meneveau. Optimal turbine spacing in fully developed wind farm boundary layers. *Wind Energy*, 15:305 – 317, 03 2012.

[15] Luke Myers and AbuBakr Bahaj. Experimental analysis of the flow field around horizontal axis tidal turbines by use of scale mesh disk rotor simulators. *Ocean Engineering*, 37:218–227, 02 2010.

[16] Ingrid Neunaber. *Stochastic investigation of the evolutoon of small-scale turbulence in the wake of a wind turbine exposed to diffeent inflow conditions*. PhD thesis, Carl von Ossietzky Universitat Oldenburg, 11 2018.

[17] Fabio Pierella and Lars Sætran. Effect of initial conditions on flow past grids of finite extension. *17th Australasian Fluid Mechanics Conference 2010*, 01 2010.

[18] P. Sforza, P. Sheerin, and M. Smorto. Three-dimensional wakes of simulated wind turbines. *Aiaa Journal - AIAA J*, 19:1101–1107, 09 1981.

List of Acronyms

AD Actuaor disk. 3, 11, 13–18, 20, 23, 24, 26, 27

NUD Non-Uniform Disk. 3, 15–17, 24, 26

PIV Particle Image Velocimetry. 11

RTWM Rotating wind turbine model. 11, 14, 17, 18, 20, 22–24, 27

UHD Uniform Holes Disk. 14–16, 24, 26

WTM Wind turbine model. 12, 17–19